Journal of Nuclear Materials 398 (2010) 227–231

Contents lists available at ScienceDirect

Journal of Nuclear Materials

journal homepage: www.elsevier.com/locate/jnucmat

Defect structures in nickel and SUS304SS formed by the collapse of cavitation bubbles

T. Yoshiie [a,*], K. Sato [a], Q. Xu [a], M. Komatsu [a,b], M. Futakawa [a,c], T. Naoe [a,c], M. Kawai [a,d]

[a] Research Reactor Institute, Kyoto University, Kumatori-cho, Sennan-gun, Osaka-fu 590-0494, Japan
[b] Hiroshima Institute of Technology, Saeki-ku, Hiroshima-ken 731-5193, Japan
[c] J-PARC Center, Japan Atomic Energy Agency, Tokai-mura, Ibaraki-ken 319-1195, Japan
[d] High Energy Accelerator Research Organization, Oho, Tsukuba-shi, Ibaraki-ken 305-0801, Japan

A B S T R A C T

A mercury target in high-power spallation neutron sources is subjected to pressure waves induced by a proton beam. The subsequent formation and collapse of cavitation bubbles lead to cavitation damage on the target vessel, especially the beam window. The cavitation damage in Ni and austenitic stainless steel SUS304SS were studied by using an electro-Magnetic IMpact Testing Machine (MIMTM) developed to simulate the damage. The existence of dislocations, stacking fault tetrahedra and vacancies was detected by positron annihilation lifetime measurements in Ni, and non-cellular dislocation structures were observed by transmission electron microscopy in Ni and SUS304SS. In addition, a high density of twins was observed in SUS304SS. These results were compared with those of high-speed compression tests using a high-speed projectile, proving that the cavitation damage caused by MIMTM corresponded to high-speed deformation.

1. Introduction

In high-power pulsed spallation neutron sources, liquid mercury is used as spallation material and coolant. It has been suggested that the intense pressure waves produced by the proton spallation reaction in the mercury target lead to cavitation in liquid mercury [1–5]. The collapse of cavitation bubbles results in erosion (pitting) of the target vessel, especially the proton beam window.

Erosion is caused by the removal of solids. Before mass decrease, plastic deformation and fatigue occur. The deformation of crystalline metals usually involves dislocations and twins. Observing the defect structural evolution will help us to understand the mechanism of the deformation and subsequent erosion.

The off-line magnetically driven impact test device electro-Magnetic IMpact Testing Machine (MIMTM) has been developed to simulate the pressure waves induced by the proton bombardment of mercury to characterize the cavitation damage on the target vessel [6–8].

In this study, we employed transmission electron microscopy (TEM) and positron annihilation lifetime measurements to characterize the cavitation damage induced in Ni and austenitic stainless steel SUS304SS by MIMTM. TEM allowed the defect structures to be observed directly. Defects that are not detectable by TEM can be detected through positron annihilation measurements.

The defect structures depend on the deformation mode [9] and deformation speed [10]. It is highly likely that the cavitation damage corresponds to high-speed deformation since calculations yielded a mercury jet speed of 300 m/s [6]. Thus, the defect structures were also compared with results of high-speed compression tests using a high-speed projectile [10] and low-speed compression tests.

2. Experimental procedure

The specimens used were Ni (99.99%) and SUS304SS. They were fabricated into discs, 3 mm in diameter and 0.1 mm in thickness. Semicircular specimens were also made by cutting discs into two. After the fabrication, the specimens were fully annealed in a vacuum. The impact test by MIMTM was performed at 560 W, 25 Hz and ambient temperature, which induced a damage corresponding to that obtained under a 1-MW proton beam injection [8]. Two types of impact tests were performed: (i) cavitation damage perpendicular to the disc as shown in Fig. 1(a), to observe it along the impact direction by conventional TEM and to perform positron annihilation lifetime measurements; (ii) cavitation damage parallel to the semicircular specimen as shown in Fig 1(b), to characterize it by cross-sectional TEM.

High-speed compression tests were performed by using a projectile having a flat hardened-steel button accelerated by compressed air through an acceleration tube as shown in Fig. 2. The maximum speed was about 100 m/s. A stopper ring was placed

* Corresponding author. Tel.: +81 72 451 2473; fax: +81 72 451 2620.
E-mail address: yoshiie@rri.kyoto-u.ac.jp (T. Yoshiie).

0022-3115/$ - see front matter © 2009 Elsevier B.V. All rights reserved.
doi:10.1016/j.jnucmat.2009.10.036

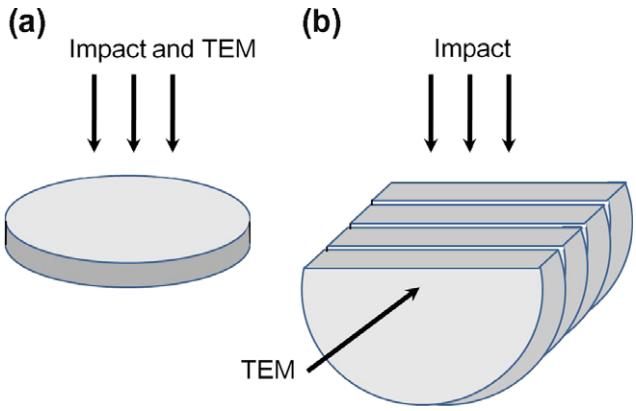

Fig. 1. Schematic illustration of two types of impact tests. (a) Cavitation damage parallel to a disc specimen for normal TEM, (b) cavitation damage perpendicular to semicircular specimens for cross-sectional TEM.

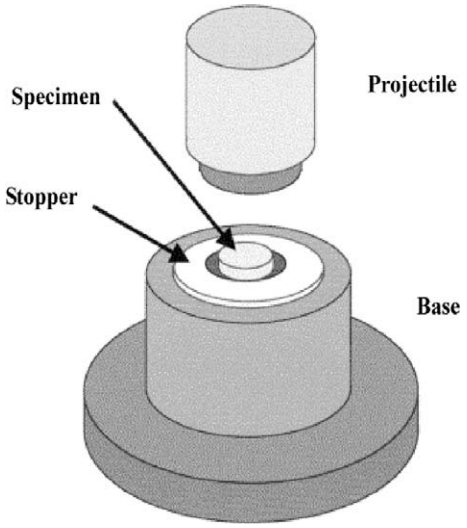

Fig. 2. Setup of specimens for high-speed compression tests.

around the specimen in order to stop the projectile abruptly so as to obtain the desired amount of deformation. In this study, 0.1-mm-thick specimens were used. A 0.07-mm-thick stopper was employed to obtain 30% deformation.

After the impact test and high-speed compression test, positron annihilation lifetime measurements using Na-22 at room temperature and conventional TEM with an acceleration voltage of 200 kV were performed. The positron lifetime measurement had a time resolution of 190 ps (FWHM) and each spectrum was accumulated to a total of over 1×10^6 counts. To discriminate between bulk and defect components, the lifetime spectrum was decomposed into two components based on the two-state trapping model after subtracting the radioactive source and background components.

The surface morphology of damaged area was observed and profiles of pits were measured by a laser microscope (Keyence VK-9510).

3. Results and discussion

3.1. Nickel

Several pits were formed by the impact test by MIMTM. Figs. 3 and 4 show damage structures on Ni surfaces observed by the laser microscope after 1000 and 2000 impacts, respectively. With increasing the number of impacts, the number of shallow pits increased and deep pits were formed. These results indicated that shallow pits were formed by a single event and deep pits were formed by a superposition of events.

Positron annihilation lifetimes of Ni are shown in Table 1. In Ni, the lifetimes of the matrix, mono-vacancies, di-vacancies and four-vacancies are 100, 169, 188 and 246 ps, respectively [11]. With increasing impact, the mean lifetime increased. Two-component lifetime analysis indicated the existence of dislocations and/or stacking fault tetrahedra [12] by 1000 impacts and mono-vacancy size defects at 2000 impact. Ni^* was measured from the backside of the impact surface. Positrons from Na-22 in metals with many defects do not migrate as long as in well-annealed metals. Therefore, it is even possible to measure the lifetime of defects distributed within 10 μm from the surface [13]. The lifetimes measured from the two surfaces were nearly the same, which indicated that the

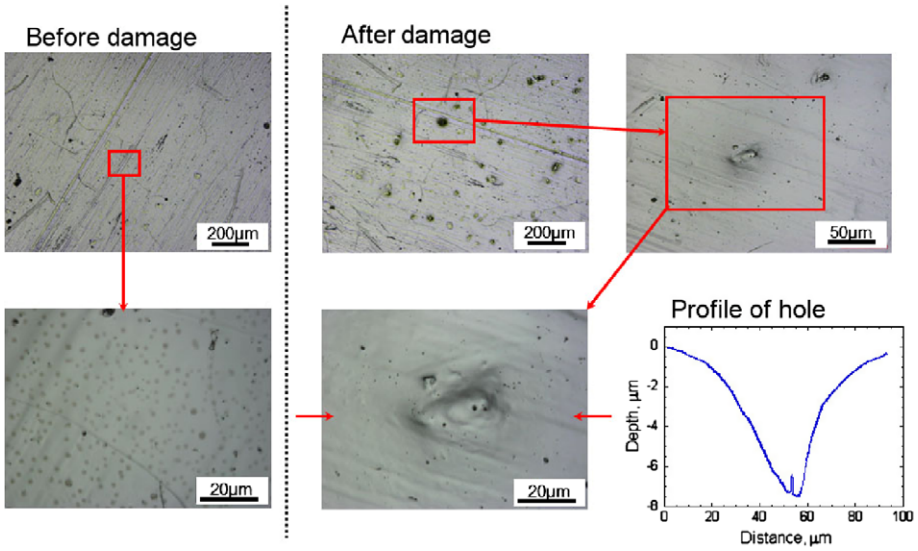

Fig. 3. Surface structures on Ni before and after 1000 impacts at 560 W and 25 Hz.

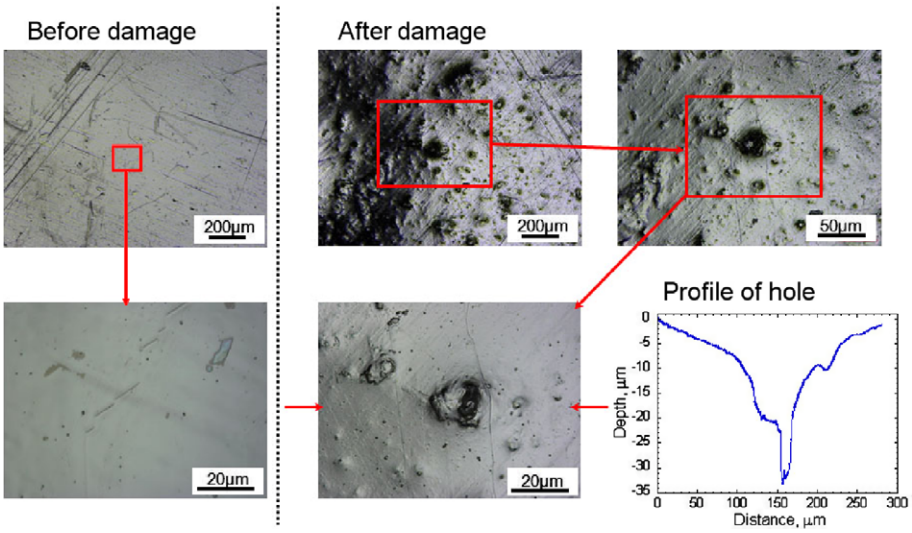

Fig. 4. Surface structures on Ni before and after 2000 impacts at 560 W and 25 Hz.

Table 1
Positron annihilation lifetime of impact-tested Ni by MIMTM and cold-rolled Ni**. Ni* was measured from the backside of the impact surface.

Specimen (impacts)	Mean lifetime (ps)	Short lifetime (ps)	Long lifetime (ps)	Intensity (%)
Ni (1000)	125.6 ± 0.4	79.2 ± 12.4	143.9 ± 6.9	54.1 ± 8.3
Ni*(2000)	131.6 ± 0.5	100.2 ± 14.5	160.7 ± 16.6	38.9 ± 17.6
Ni**(2000)	133.3 ± 0.4	99.3 ± 9.3	168.3 ± 11.1	38.2 ± 10.1
Ni**	134.6 ± 0.5	117.6 ± 3.0	235.1 ± 18.6	10.7 ± 2.7

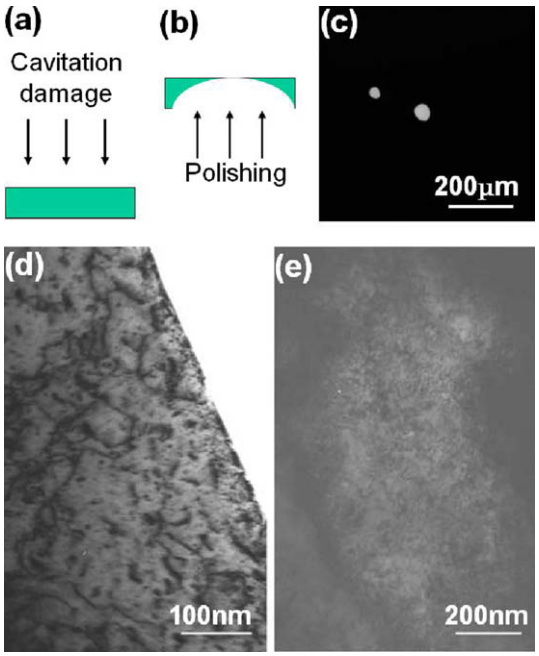

Fig. 5. Defect structures near the surface on Ni after 1000 impacts at 560 W and 25 Hz. (a) Schematic illustration of disc and damage, (b) backside polishing, (c) low-magnification photo after backside polishing, (d) peripheral hole and (e) thin area just before hole formation.

cavitation damage formed not only near the impact surface, but rather was homogeneously distributed over the 0.1-mm-thick specimen.

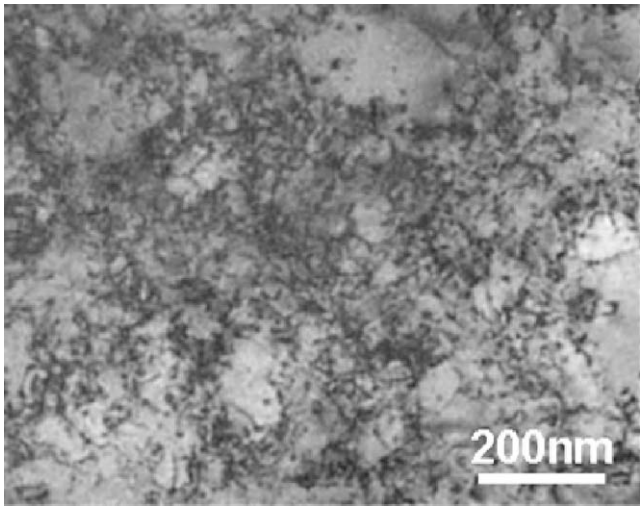

Fig. 6. Defect structure in Ni after high-speed compression testing at a projectile speed of 100 m/s.

In Table 1, the lifetime of cold-rolled specimens is also presented as a comparison. The choice of 300% deformation was to obtain almost the same mean lifetime as 2000 impacts. Though the mean lifetime was almost the same, the long lifetime was different between MIMTM impact testing and cold rolling. The formation of microvoids of four vacancies [12] was caused by localized generation of vacancies such as rows of vacancies being created by moving jogs on dislocations. The difference suggests that the impact test by MIMTM produces mainly isolated mono-vacancies different from the plastic deformation due to the generation and movement of dislocations.

Impact-tested specimens were characterized by TEM. After impact testing (Fig. 5(a), specimens were polished on the backside (Fig. 5(b) to observe near the impact surface. After the formation of small holes, as shown in the low-magnification micrograph in Fig. 5(c), the polishing was stopped. At this stage, thin areas of peripheral holes (Fig. 5(d) and a very thin area about to become a hole (Fig. 5(e) were observed. In both cases, very fine dislocation structures were observed. In Ni, dislocations are usually distributed heterogeneously, forming dislocation cells (cellular structure) after deformation, as discussed later in Fig. 6. After impact testing, however, dislocations were distributed homogeneously.

Fig. 6 shows the results of high-speed compression tests using a projectile speed of 100 m/s. The dislocation structure was also fine but heterogeneously distributed, making the cellular structure different from that obtained through impact testing. According to Kiritani et al. [10], the cell size in Ni decreased with increasing projectile speed. In the case of Al, the cellular structure changed into a homogeneous random distribution of dislocations with increasing projectile speed.

It was concluded that the deformation speed induced by impact testing was higher than that obtained by high-speed compression testing with a projectile speed of 100 m/s. The calculation that yielded a mercury jet speed of 300 m/s [6] was supported by the defect structures. Kiritani has proposed a high-speed deformation mechanism and the direct formation of vacancies and vacancy clusters [14]. Vacancies and stacking fault tetrahedra detected by positron annihilation lifetime measurements may be formed by his mechanism.

3.2. Austenitic stainless steel

Cross-sectional TEM observation of the deformed structures in SUS304 SS was performed. A bundle of specimens as illustrated in Fig. 1(b) was damaged to fabricate cross-sectional TEM speci-

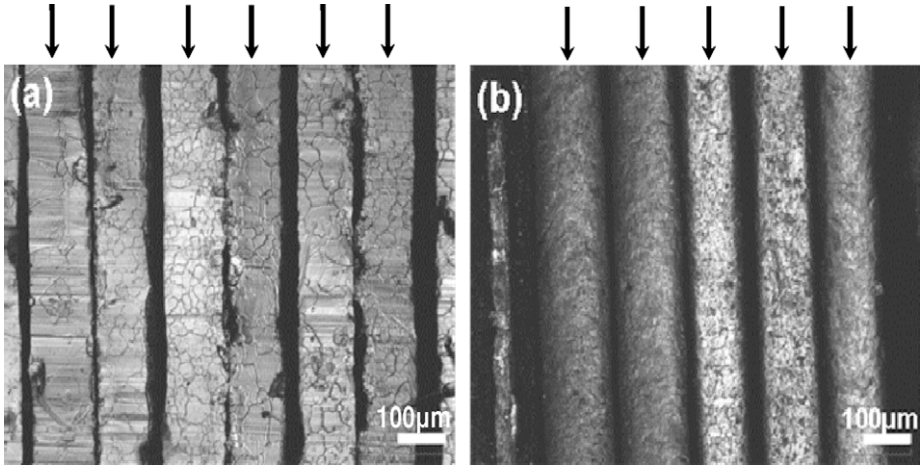

Fig. 7. Surface damage structures of specimens before (a) and after (b) an impact test at 560 W and 25 Hz, for the observation of cross-sectional TEM. Each arrow indicates each specimen.

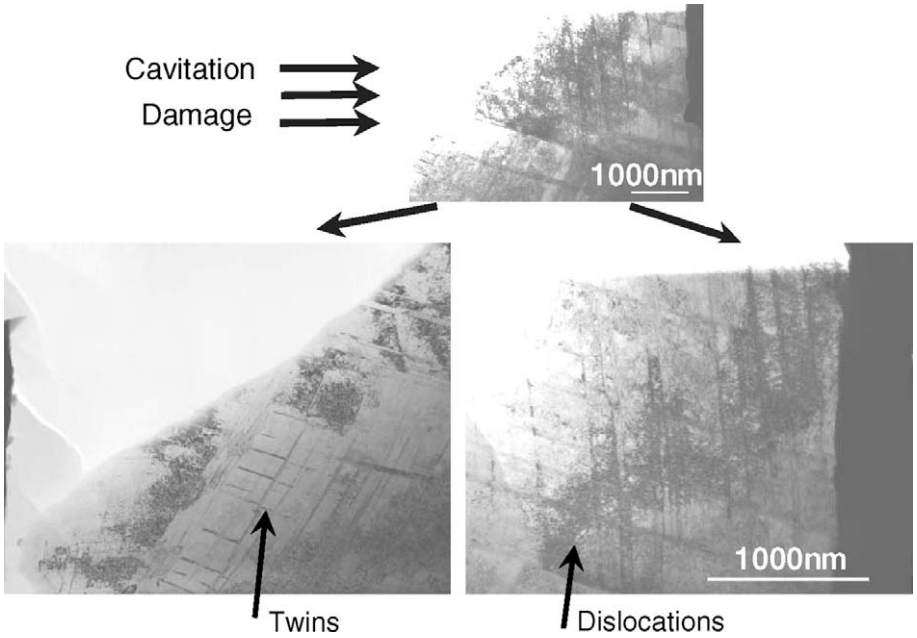

Fig. 8. Cross-sectional TEM of SUS304SS after an impact test at 560 W and 25 Hz. Low magnification (upper photo) and high magnification (lower photos). Twins and dislocation rich area are indicated by arrows.

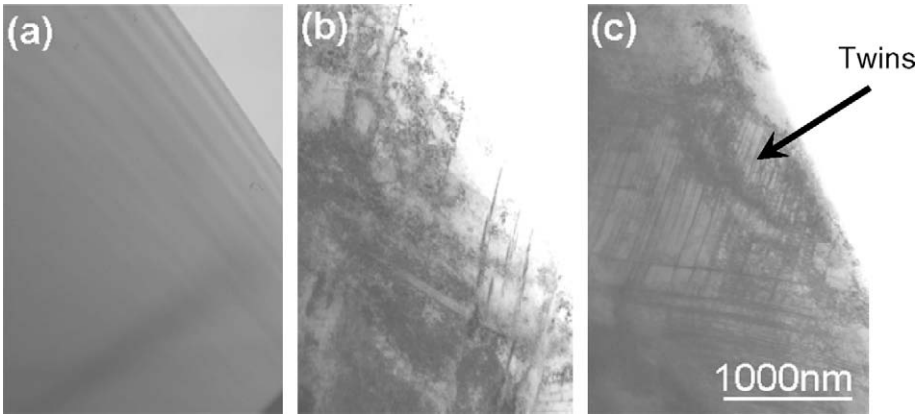

Fig. 9. Defect structure in SUS304SS before (a) and after high-speed compression testing at a projectile speed of 44 m/s (b) and 95 m/s (c). Twins are indicated by an allow.

men easily. The specimen surface morphology change observed by the laser microscope before and after impact testing is shown in Fig. 7. During these tests, specimens fell out of the holder and so accurate impact results could not be obtained. On the basis of the surface change, however, they were estimated to be around 1000 impacts. In addition to dislocations, many twins were observed, as shown in Fig. 8. As in the case of Ni, no clear cellular structures were observed.

Fig. 9 shows the defect structures after high-speed compression tests using projectile speeds of 44 and 95 m/s. With increasing deformation speed, the density of twins increased and the cell size decreased. The defect structures, density of twins and dislocation structures for the impact test and high-speed compression test clearly revealed that SUS304SS underwent high-speed deformation during the impact tests.

4. Concluding remarks

Cavitation damage structures induced by MIMTM were studied through positron annihilation lifetime measurement and TEM. The results revealed a very fine non-cellular dislocation structure in Ni and a very fine non-cellular dislocation structure with twins in SUS304SS. These findings indicated that the cavitation damage induced by MIMTM corresponded to high-speed deformation. These were the results for a single event or several superposed events before the occurrence of erosion. In order to elucidate the erosion mechanism to predict the lifetime of the target and for materials development to reduce the damage on the spallation window, more research into higher number of impacts is required.

Acknowledgements

This work was supported by JSPS, Grant-in-Aid for Science Research (S), Task No. 19106017, and by the sponsorship of JNES open application research project for enhancing the basis of nuclear safety.

References

[1] M. Futakawa, T. Naoe, C.C. Tsai, H. Kogawa, S. Ishikura, Y. Ikeda, H. Soyama, H. Date, J. Nucl. Mater. 343 (2005) 70.
[2] Y. Ikeda, J. Nucl. Mater. 343 (2005) 7.
[3] J.R. Haines, B.W. Riemer, D.K. Felde, J.D. Hunn, S.J. Pawel, C.C. Tsai, J. Nucl. Mater. 343 (2005) 58.
[4] M. Futakawa, T. Naoe, H. Kogawa, C.C. Tsai, Y. Ikeda, J. Nucl. Sci. Technol. 40 (2003) 895.
[5] B.W. Riemer, J.R. Haines, J.D. Hunn, D.C. Lousteau, T.J. McManamy, C.C. Tsai, J. Nucl. Mater. 318 (2003) 92.
[6] M. Futakawa, T. Naoe, H. Kogawa, H. Date, Y. Ikeda, JSME A48 (2005) 234.
[7] M. Ida, T. Naoe, M. Futakawa, Phys. Rev. E 75 (2007) 046304.
[8] M. Futakawa, H. Kogawa, S. Hasegawa, Y. Ikeda, B. Riemer, M. Wendel, J. Haines, G. Bauer, T. Naoe, K. Okita, A. Fujiwara, Y. Matsumoto, N. Tanaka, J. Nucl. Mater. 377 (2008) 182–188.
[9] K. Sato, M. Kai, K. Mitima, Q. Xu, T. Yoshiie, Phys. Stat. Sol. c4 (2007) 3559–3562.
[10] M. Kiritani, T. Sota, T. Tawara, H. Arimura, K. Yasunaga, Y. Matsukawa, M. Komatsu, Rad. Effect. Defect. Sol. 157 (2002) 53.
[11] H. Ohkubo, Z. Tang, Y. Nagai, M. Hasegawa, T. Tawara, M. Kiritani, Mater. Sci. Eng. A350 (2003) 95.
[12] E. Kuramoto, T. Tsutsumi, K. Ueno, M. Ohmura, Y. Kaminura, Comput. Mater. Sci. 14 (1999) 28.
[13] T. Ishizaki, Q. Xu, T. Yoshiie, N. Nagata, Mater. Trans. 45 (2004) 9–12.
[14] M. Kiritani, K. Yasunaga, Y. Matsukawa, M. Komatsu, Rad. Eff. Def. Sol. 157 (2002) 3.